

Monitoring of bridge overlay using shrinkage-modified high performance concrete based on strain and moisture evolution

Yifeng Ling^{*1}, Gilson Lomboy², Zhi Ge¹ and Kejin Wang^{**3}

¹Department of Qilu Transportation, Shandong University, Jinan 250002, Shandong Province, PR China

²Department of Civil and Environmental Engineering, Rowan University,
201 Mullica Hill Road, Glassboro, NJ 08028, USA

³Department of Civil, Construction and Environmental Engineering, Iowa State University,
Ames, IA, 50011, USA

(Received May 5, 2022, Revised May 30, 2023, Accepted June 7, 2023)

Abstract. High performance concrete (HPC) has been extensively used in thin overlay for repair purpose due to its excellent strength and durability. This paper presents an experiment, where the sensor-instrumented HPC overlays have been followed by dynamic strain and moisture content monitoring for 1 year, under normal traffic. The vibrating wire and soil moisture sensors were embedded in overlay before construction. Four given HPC mixes (2 original mixes and their shrinkage-modified mixes) were used for overlays to contrast the strain and moisture results. A calibration method to accurately measure the moisture content for a given concrete mixture using soil moisture sensor was established. The monitoring results indicated that the modified mixes performed much better than the original mixes in shrinkage cracking control. Weather condition and concrete maturity at early age greatly affected the strain in concrete. The strain in HPC overlay was primarily in longitudinal direction, leading to transverse cracks. Additionally, the most moisture loss in concrete occurred at early age. Its rate was very dependent on weather. After one year, cracking survey was carried out by vision to verify the strain direction and no cracks observed in shrinkage modified mixes.

Keywords: dynamic moisture content; high performance concrete (HPC); overlay condition monitoring; soil moisture sensor; strain direction

1. Introduction

High performance concrete (HPC) is increasingly used in bridge deck overlays for pavement repair because of its high strength, low permeability and excellent durability. However, due to its high cementitious content, low water-to-binder ratio (w/b), and use of various admixtures, HPC is also reported to have a high risk for shrinkage cracking (Wu *et al.* 2017, Wang *et al.* 2013, Yuan *et al.* 2018, Ma *et al.* 2018, Afroughsabet *et al.* 2020). Shrinkage in HPC can be mainly affected by concrete mix design, ambient temperature, moisture content and the saturation level of underlying

*Corresponding author, Professor, E-mail: yfling@sdu.edu.cn

**Corresponding author, Professor, E-mail: kejinw@iastate.edu

^aProfessor

^bProfessor

layers (Rao and Roesler 2005, Shen *et al.* 2018, Ray *et al.* 2012, Shen *et al.* 2018). Differential moisture content and ambient temperature causes shrinkage in concrete due to volume change as a result of moisture loss from the concrete surface (Hansen and Wei 2008, Dong *et al.* 2019). The total moisture loss can be seen as a result of drying shrinkage (Hansen and Wei 2008, Wei and Hansen 2011, Wu *et al.* 2022) which is due to the evaporation of capillary water near the surface. Adding shrinkage reducing admixture and reducing cementitious materials are commonly used to control HPC shrinkage in construction engineering (Klausen and Kanstad 2020, James and John 2020, Chung *et al.* 2020).

For cost consideration, the performance and condition of thin HPC overlays needs field continuously investigation especially for strain and moisture level in concrete, which demands reliable sensors. The strain measured in a length of concrete is the ratio of the change in length under applied load divided by the original length. Pavement deformation is captured by concrete strain measurements to evaluate the deformation or the change in the pavement's profile. Deformations can either be elastic (temporary) or plastic (permanent). However, concrete pavement is considered to not have permanent deformations or rutting like asphalt pavement does. The temperature gradient within the slab due to seasonal and daily variations in temperature results in expansion of the concrete. These volume changes and deformations can create critical stresses which may result in joint spalling and cracks (Rice 2014). Therefore, the strain and moisture monitoring are main concerns as concrete overlay durability.

In recent years, pavement instrumentation has become an important aid-tool of pavement monitoring, for the assessment of pavement structural behavior. Parameters measured on site are mainly: strain, temperature, and moisture. Vibrating wire sensors have been successfully used to monitor pavement behavior such as the total strain caused by concrete shrinkage, traffic loading and environment (Barroca *et al.* 2013, Buenfeld *et al.* 2008, Mccarter and Vennesland 2004, Bahrani *et al.* 2020). Further, long-term monitoring data can improve modeling and analytics resulting in prolonged structure service life and reduced life cycle costs. Ni *et al.* developed a model for long-term performance of concrete bridge which accurately predicted the service life of structure (Ni 2005). Elyas *et al.* trained a model based on the data from long-term structural monitoring to effectively evaluate mechanical performance of bridge overlay (Elyas 2018). Whereas, moisture sensors (MS) have not been applied to monitor the internal dynamic moisture content of concrete accurately. Numerous studies have been conducted to express relative humidity in concrete as an index for moisture content in concrete (Norris *et al.* 2008, Yang *et al.* 2015, Min *et al.* 2018). However, the relative humidity can't address water proportion in concrete, instead only shows the ratio of the partial pressure of water vapor to the equilibrium vapor pressure of water at a given temperature. It would not help monitor the concrete condition in particular structure.

In this paper, concrete overlay condition (strain and moisture) was monitored accurately for 1 year using vibrating wire and soil MS. Meanwhile, an innovative methodology to monitor dynamic moisture content in concrete overlay was developed by calibration for a given concrete mixture. Relationships between strain/moisture in concrete and ambient temperature were discussed. Dynamic behaviors of strain and moisture at different locations of bridge overlay were revealed. Additionally, the strain direction in concrete overlay was also detected.

2. Field preparation

Table 1 Mix proportions of HPC

Mix	SR L/m ³	Cement kg/m ³	C-FA kg/m ³	GGBFSkg/m ³	Limestone kg/m ³	Sand kg/m ³	Water kg/m ³	w/b
6	-	489.7	-	-	822.5	810.2	160.1	0.33
6-SR1.0	5.0	489.7	-	-	822.5	810.2	160.1	0.33
8	-	218.3	79.4	99.2	848.9	833.5	158.8	0.40
8-CM90	-	203.0	73.8	92.2	876.9	861.1	147.6	0.40



Fig. 1 The US 20 over I 35 dual bridge location

2.1 Numerical simulation procedure

The HPC mixes used in the field were Mix 6, Mix 6-SR1.0, Mix 8, and Mix 8-CM90. Their proportions are listed in Table 1. Mix 6 was identified as a high cracking potential mix (Wang et al. 2013). It was made with 489.7 kg/m³ of Type I cement and a low w/b of 0.33. In order to reduce shrinkage of this mix with proper workability, shrinkage reducing admixture (SR) was added into the mixture named as Mix 6-SR1.0 at 5 L/m³ (1.0 gallon/cy) dosage.

Mix 8 was identified as a medium cracking potential mix (Wang *et al.* 2013). It was made with 55% Type I cement, 20% of Class C fly ash (FA) and 25% of ground granulated blast-furnace slag (GGBFS) at a binder content of 396.8 kg/m³ and a w/b of 0.40. In order to reduce shrinkage of this mix, cementitious material or binder content of this mix was reduced to 90% coined as Mix 8-CM90.

2.2 Site selection

As shown in Fig. 1, field site was selected on the US 20 over I 35 dual bridge in Iowa, where four HPC mixes, namely Mix 6 and Mix 6-SR1.0 as well as Mix 8 and Mix 8-CM90 were placed side-by-side for the bridge overlays. The bridge is in the east-west direction. Because these new overlays were in similar geometries, restraints, environmental exposure, and traffic loads, their performance could be monitored and compared more accurately.

Table 2 The US 20 over I 35 construction timeline

Date	Activity
7/21/2016	Installed sensors on West Bound, Stage 1, part 2 (Mix 6 overlay)
7/22/2016 (Day 0)	Placed Mix 6 concrete overlay on West Bound, Stage 1, part 2
7/27/2016	Installed sensors on East Bound, Stage 1, part 2 (Mix 8 overlay)
7/28/2016 (Day 6)	Placed Mix 8 concrete overlay on East Bound, Stage 1, part 2
8/26/2016	Installed sensors on West Bound, Stage 2 (for Mix 6M or 6-SR1.0 overlay)
8/29/2016 (Day 38)	Placed Mix 6-SR1.0 concrete overlay on West Bound, Stage 2
8/31/2016 (Day 40)	Installed sensors on East Bound, Stage 2, and also placed Mix 8M or 8-CM90 concrete overlay on East Bound, Stage 2

(Day 0 indicates the starting day of sensor monitoring)

As shown in Fig. 1, each of the dual bridge was 79 m long and 15 m wide. It has two stages for construction: Stage 1 is outside (slower traffic) the bridge and Stage 2 is inside (faster traffic) the bridge. Mix 6 (original and modified) and Mix 8 (original and modified) were placed on the westbound and eastbound bridge deck, respectively. Mix 6 and Mix 8 were paved in Stage 1, while Mix 6-SR1.0 and Mix 8-CM90 were paved in Stage 2. The thicknesses of the new concrete overlays were all 5 cm. Table 2 shows the construction timeline related to the present field study.

3. Health monitoring system

3.1 Sensors description and location

A total of 33 sensors, including MS, Type T thermocouple, and strain gauges were employed in this study.

(1) MS

The Decagon GS3 was adopted for moisture monitoring due to its high stability and durability in concrete as seen in Fig. 2. It has a microprocessor to measure the charge and an electromagnetic field to output the dielectric permittivity of the surrounding medium. However, the default equation for soil must be calibrated to convert dielectric value to water content for concrete use.

(2) Strain gages

Geokon Model 4200 vibrating wire strain gauge (Fig. 3), designed for direct embedment in concrete was used considering its excellent long-term stability, high water resistance, and a frequency output suitable for transmission over very long cables. The strain in concrete can be determined by plucking the wire and measuring its resonant frequency of vibration.



Fig. 2 GS3 MS



Fig. 3 Model 4200 Geokon strain gauge

Table 3 Sensors location in overlay

Location	Distance from abutment	Direction	Sensor type	Westbound		Eastbound	
				Stage1	Stage 2	Stage 1	Stage 2
1	0.9 m	Transverse	Geokon 4200	VB2	VB8	VB 24	VB16
		Transverse	Geokon 4200	VB3	VB9	VB25	VB17
2	7.2 m	Longitudinal	GS3	MS1	MS3	MS7	MS5
		Transverse	Geokon 4200	VB4	VB10	VB26	VB18
3	18.6 m	Transverse	Geokon 4200	VB5	VB11	VB27	VB19
		Transverse	Geokon 4200	VB6	VB12	VB28	VB20
4	22.7 m	Longitudinal	GS3	MS2	MS4	MS8	MS6

Note: VB denotes vibrational strain gauge sensor and MS denotes moisture sensor

(3) Location of sensors

20 strain gauges and 8 MSs were embedded at the depth of 2.5 cm in the new overlays from the edges of the abutment to the middle point between pier 1 and pier 2. The locations, orientation, and layouts of the sensors are shown in Fig. 4. On the stage 1-part 2 and stage 2 of each bridge, 4 strain gauges were installed transversely at 0.9 m, 7.2 m, 18.6 m and 22.7 m respectively, and one was installed longitudinally at 22.7 m from the abutment. 2 MSs were installed at 7.2 m and 22.7 m from the abutment, respectively.

Additionally, a mini slab were cast in the field for all mixes, with a strain gauge embedded to measure the strain from free shrinkage. The detailed information of mini slabs is in section 4. The identifications of the sensors in overlay are listed in Table 3.

(1) Procedures of installation

The installation of sensors was completed prior to concrete paving. As shown in Fig. 5, each strain gauge was fixed at 2.5cm high on the substrate by 2 screwed plastic seats. The MS was supported also at 2.5 cm in height using glue and screws.

It should be noted that, during the installation of the sensors, the sensors and wires needed extra attention because there would be very difficult to repair them once they were cast inside concrete. In this research, all wires were went through the deck, and placed in a polyvinyl chloride (PVC) pipe under bridge as seen in Fig. 6(a), to connect with data acquisition system (DAS) stored in an alloy shield box. To avoid wire mess, zip ties were used to mount extra wires to PVC pipe. A thermal couple was attached under the concrete deck above the DAS to record ambient temperature as shown in Fig. 6(b).

(2) DAS

As shown in Fig. 7, DAS includes one Campbell CR1000 data logger, three AM16/32B-ST-SW multiplexers, one vibrating wire analyser module (AVW200), one solar panel, and one battery used for data collection. DAS was fixed on girder above the ground to reduce environmental

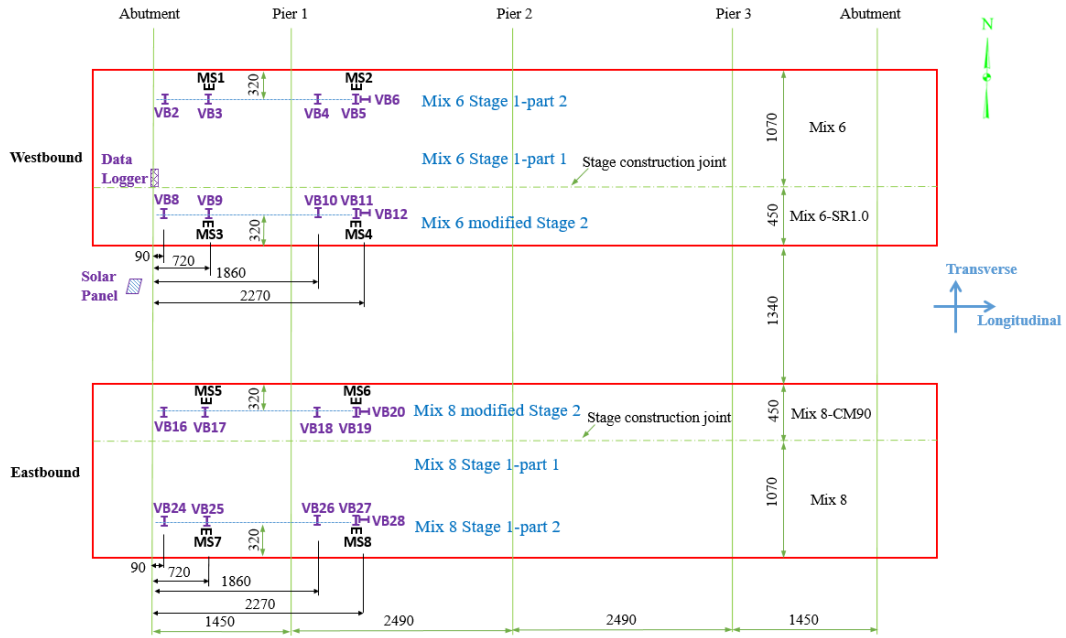
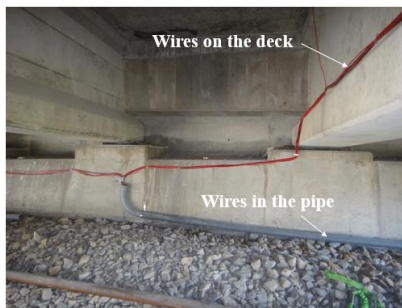


Fig. 4 Sensors location on the bridge deck (unit in cm)



Fig. 5 Installation of Geokon4200 and GS3 on deck



(a) Wires in PVC pipe



(b) Wires to DAS

Fig. 6 Wires layout

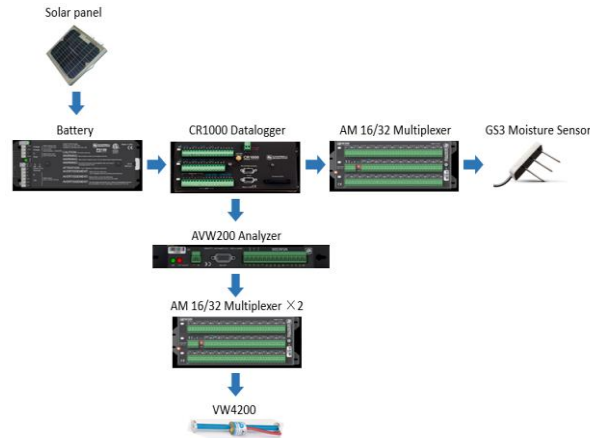


Fig. 7 Data acquisition system



(a) Concrete in sealed bags



(b) Concrete cylinder with MS

Fig. 8 Concrete samples used for MS calibration

disturbances. The solar panel in an open area between the east and west bound bridges, continuously supplied power of DAS through a 12 V battery source. The data logger was connected with a multiplexer for MSs, and an AVW200 which was extended for two AM16/32 multiplexers for stain gauges as shown in Fig. 8. In this study, the sensor readings were recorded every 5 minutes, and the total monitoring time was about one year.

3.2 MS calibration

The GS3 MS has a generic equation (Eq. (1)) to calculate volumetric water content (VMC) with an accuracy of 5% for potting soil, perlite and peat, calibrated by the manufacturer as seen below.

$$\text{VWC}\left(\frac{m^3}{m^3}\right) = 5.89 \times 10^{-6} \varepsilon^3 - 7.62 \times 10^{-4} \varepsilon^2 + 3.67 \times 10^{-2} \varepsilon - 7.53 \times 10^{-2} \quad (1)$$

Where ε is dielectric permittivity measured directly by the sensor.

However, the above default equation is not suitable for concrete due to various mix proportions.

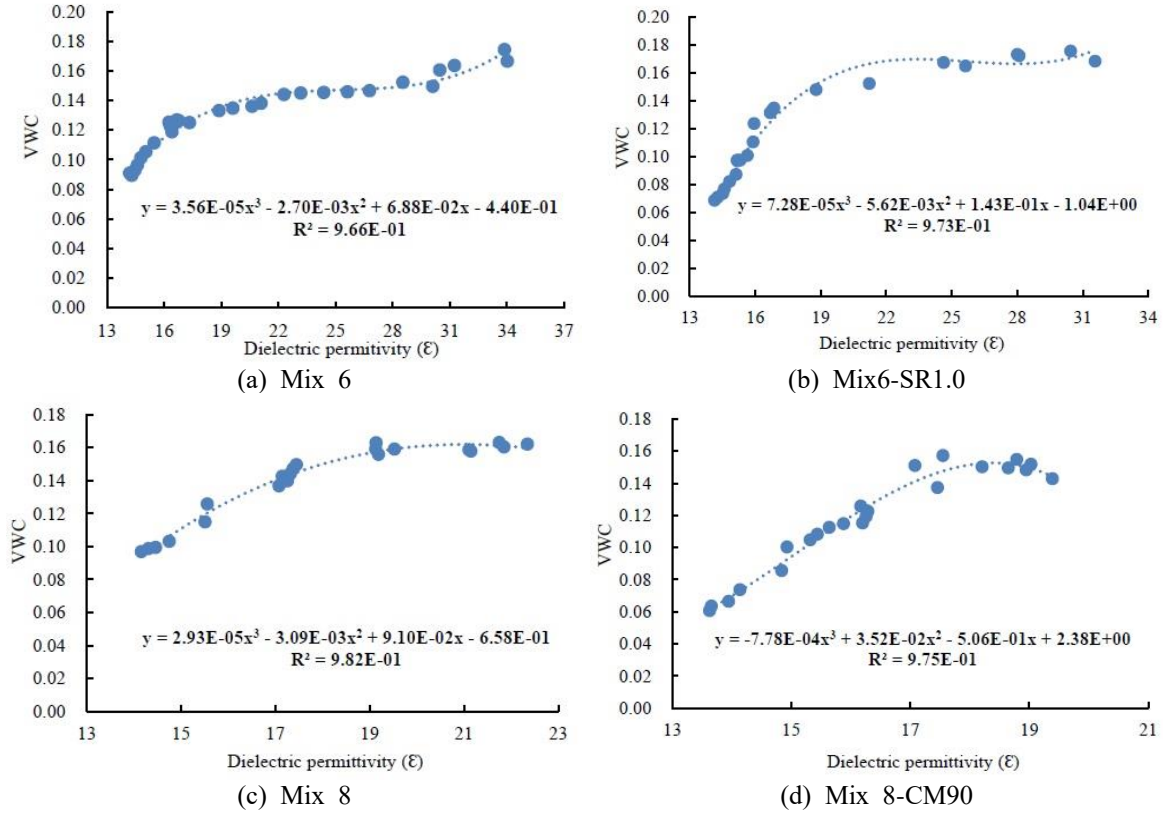


Fig. 9 Calibrated VWC equations for four mixes

Thus, it had to be calibrated for each concrete mix. The basic principle of calibration for concrete was to measure VMC and ϵ over time in concrete under similar condition to the field. Then, a polynomial trend line of VMC- ϵ was regressed similar to the above default equation, for the concrete mix.

For each mix, after mixing, 17 bags of concrete with the same volume of 400 cm^3 and a $10 \times 20 \text{ cm}$ cylinder were cast. They were completely sealed with plastic sheet to simulate the field concrete curing under burlap. After designated time interval, the water content of the concrete in each bag was determined by the weight loss of concrete in each bag using microwave drying after different curing time, as seen in Fig. 8(a). Meanwhile, ϵ of concrete was recorded by a MS inserted to the concrete cylinder, as shown in Fig. 8(b). Generally, the time interval was 1-2 hours within the first day, but larger 3-4 hours afterwards as the rate of moisture loss decreased.

After the burlap was removed from the field concrete, the concrete cylinder was demolded to determine VWC by measuring the weight loss of the cylinder daily until the age of 36 days (the calibration stopped at 36th day for each mix due to negligible weight loss). According to the test results, polynomial VWC vs. ϵ curves were fitted for all concrete mix to obtain their relationships, as shown in Figs. 9(a)-9(d). Using these equations, VWC of concrete overlays were calculated based on ϵ from the embedded sensor.



Fig. 10 (a) Mini slab mold and strain gauge location and (b) Mini slabs on the field site

3.3 Strain measurements

The strain (μ) after temperature correction could be expressed as

$$\mu = (R_1 - R_0)B + (T_1 - T_0)(C_1 - C_2) \quad (2)$$

Where R_0 is the initial reading and R_1 is the current reading of strain from the strain gage; B is the batch gage factor of 0.975; T_0 is the initial temperature and T_1 is the current temperature; C_1 is the coefficient expansion of steel and C_2 is the coefficient of expansion of concrete. It should be noted that the positive μ is tensile and the negative μ is compressive.

4. Construction and sample preparation

During overlay construction, a layer of grout was first brushed on the concrete substrates. The fresh concrete was spread on the deck by shovelling and vibrated for consolidation. Then, a paving machine stroke off extra concrete to have a uniform thickness, followed by a screed finishing. The surface was textured and cured using burlap and chemical compounds, respectively. Since paver, vibrator and heavy mass of concrete were potential threats to break either the sensors or the wires, fresh concrete was carefully pre-poured on the top of sensors to mitigate such risk.

For each field concrete mix, twelve $\Phi 102 \text{ mm} \times 203 \text{ mm}$ cylinders, three $76 \text{ mm} \times 76 \text{ mm} \times 286 \text{ mm}$ prisms and one $305 \text{ mm} \times 152 \text{ mm} \times 51 \text{ mm}$ mini slab were cast on site. All 12 cylinders were demolded after 1 day, and cured in a foggy room (25°C and $99\%\text{RH}$). Compressive strength of the cylinders was tested at 3, 7, 14 and 28 days (3 replicates for each measurement) according to ASTM C39 (2018). The prism samples cast at the field site were taken to the lab on the next day of casting, and free drying shrinkage of the samples was measured according to ASTM C 157 (2017). The mini slab aimed at investigating the difference in strain measurement between restrained concrete (overlay) and non-restrained concrete (mini slab) under the same environment.

To make a mini slab, a strain gauge was preinstalled in the middle of the slab formwork (also in the middle of the height), as shown in Fig. 10(a), before concrete casting. After casting, the mini concrete slab was cured under a wet towel and placed under the bridge. The strain gauge was connected to DAS. After 24 hours, the slab was demolded and sealed on the bottom and side surfaces, leaving only the top surface open to the environment. The slab was then moved to an open area near its corresponding concrete overlay to ensure the same weather conditions.

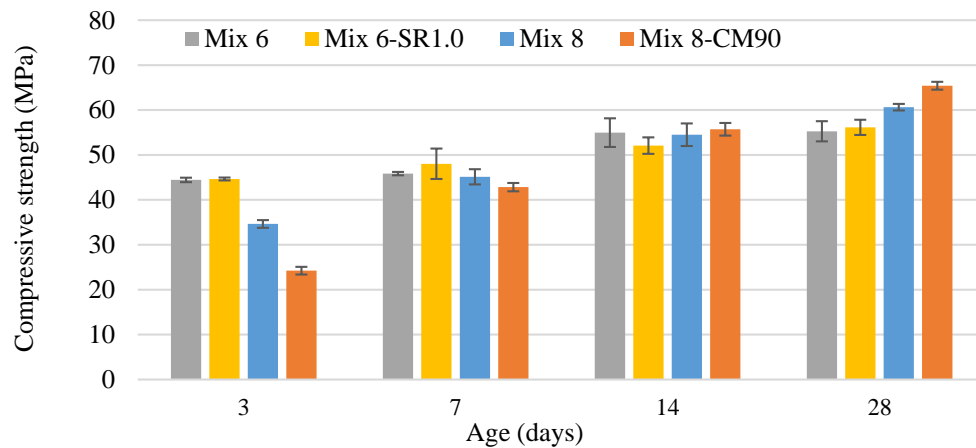


Fig. 11 Compressive strength of mixes.

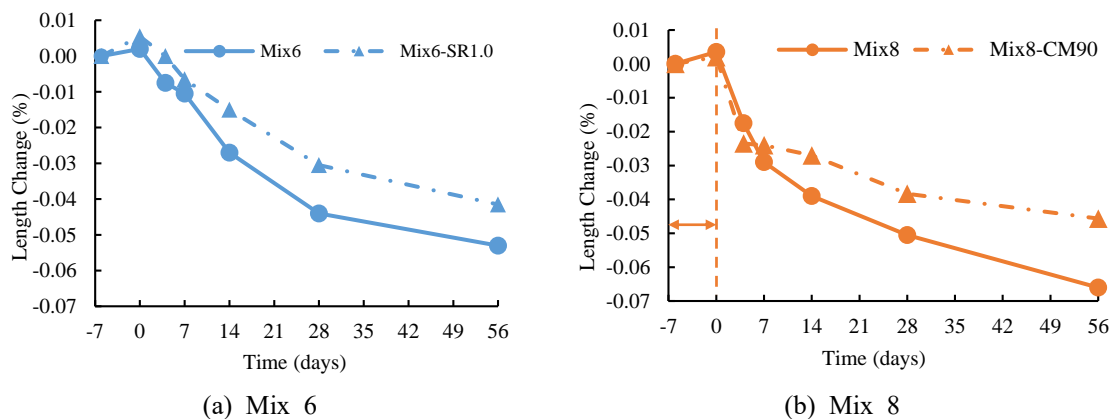


Fig. 12 Free drying shrinkage of field concrete mixes

Fig. 10(b) presents the layout of mini slabs with a wooden protection. The mini slabs of four field concrete mixes were placed together on the wooden plates that were supported by wooden bars and reinforced by a steel wire for their positions. It can be seen in Fig. 10(b) that the wires from strain gauges of the mini slabs were tied together by a tape, passed through a PVC pipe, and then connected to the data logger.

5. Results and discussion

5.1 Compressive strength

Compressive strengths of the 4 field concrete mixes (cast in field) were tested, and the results were shown in Fig. 11. It can be seen from Mix 6 that 1.0 gallon/cy (4.95 L/m³) of SR addition did

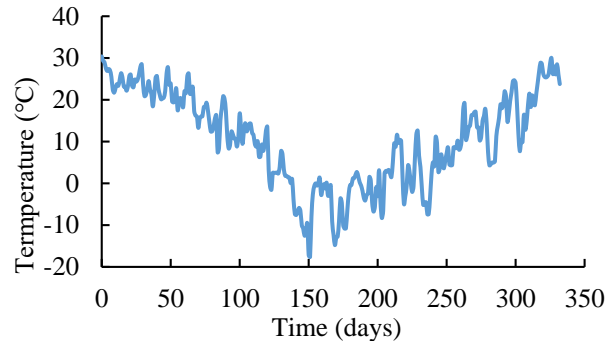


Fig. 13 Ambient temperature of the field sited (where Day 0 was on June 22, 2018, the day of the first overlay construction).

not affect the concrete compressive strength. ASTM C494 (2019) requires that mixes with special admixtures should not have less than 90% of the strength of the reference mix at the same age. Addition of 1.0 gallon/cy (4.95 L/m³) of SR in mix 6 met this criterion. For Mix 8, the 10% cementitious reduction only reduced the early age strength of field concrete; and interestingly, the 28-day strength of Mix 8-CM90 was even a little higher than that of Mix 8. This might be due to the field hot environmental temperature, which possibly accelerated both hydration and pozzolanic reaction of slag and fly ash.

5.2 Free drying shrinkage

The free drying shrinkage of field concrete samples are shown in Fig. 12. It illustrates that 4.95 L/m³ SR addition reduced the free drying shrinkage of Mix 6 by 20%, and 10% cementitious reduction decreased the free drying shrinkage of mix 8 by approximately 30%.

5.3 Field ambient temperature

The daily average ambient temperatures are shown in Fig. 13. It can be seen that the maximum (30.4°C) and minimum (-17.6°C) temperatures were observed at Day 0 (June 22, 2016) and Day 150 (November 20, 2016) respectively. The maximum difference of ambient temperature was 48.0°C in the monitoring period.

5.4 Moisture content of concrete overlays

All MSs functioned appropriately during the entire monitoring period. VWC profiles captured by the MSs were illustrated in Fig. 14. It provides a comparison of MS readings at 0, 14, 50, and >300 days after starting of the sensor monitoring. Several observations can be made from these figures:

(1) The initial VWC was about 0.15 for Mix 6 and 0.16 for the rest mixes, which was consistent with that calculated from their mix proportions. The calibrated equations are perfectly matched to their corresponding mixes.

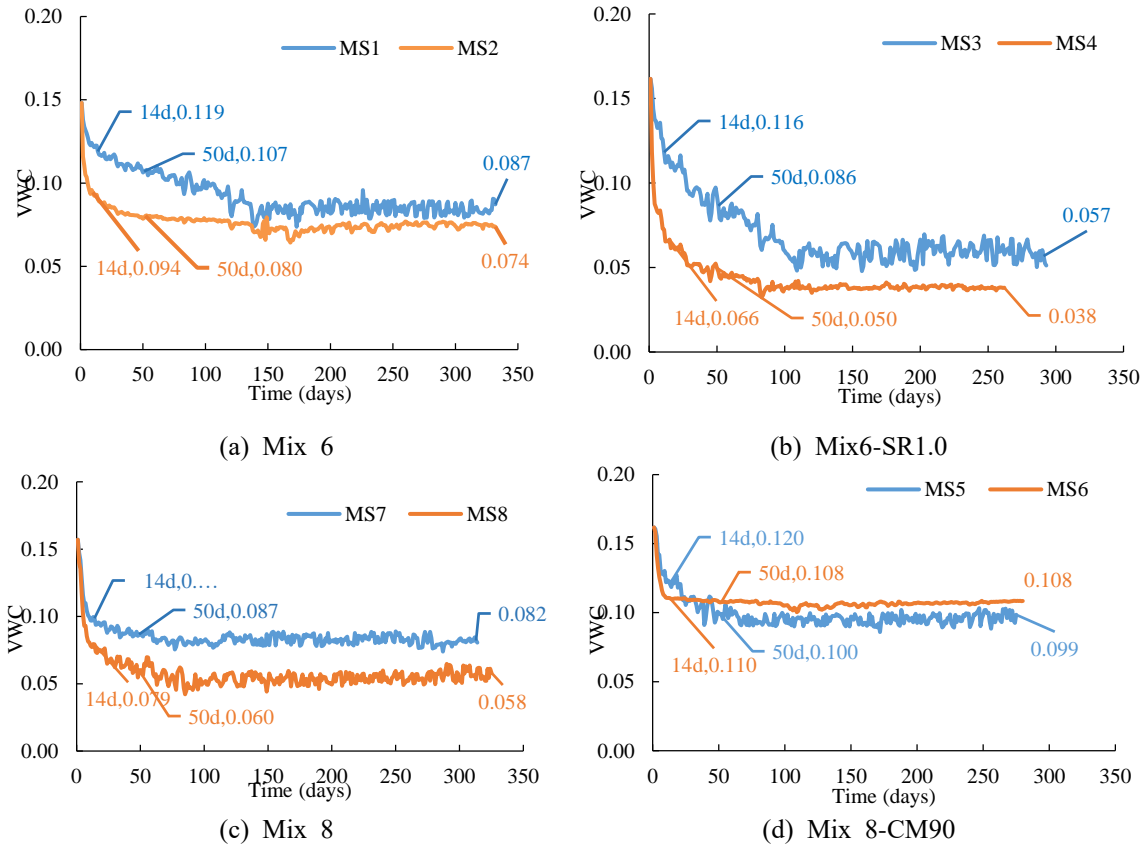


Fig. 14 VWC measurements from Mix 8 series (MS1 and 3 were 720 cm and MS 2 and 4 were 2270 cm from the abutment, MS5 and 7 were 720 cm and MS 6 and 8 were 2270 cm from the abutment)

(2) The VWC readings of MS1, 3, 5, and 7 (in blue) at the locations 720 cm from the joint (near the abutment) were generally higher than those of the MS2, 4, 6, and 8 (in orange) at the locations 2270 cm from the joint, except for Mix 8-CM90.

(3) For Mix 6 series, the VWC readings of the MS1 and 3 (in blue) close to the joint near the abutment dropped slowly to a stable VWC; while the VWC readings of MS2 and 4 (in orange) further away from the joint dropped rapidly to a stable VWC. This indicates that the joint probably allowed moisture ingress.

(4) Mix 6 reached a stable VWC at approximately the coldest day (150 days after construction), and the stable VWC values of Mix 6 were 0.087 and 0.074 for MS1 and MS2, respectively. Mix 6-SR1.0 reached a stable VWC at approximately 100 days after its overlay construction, and the stable VWC values of Mix 6-SR1.0 were 0.057 and 0.038 for MS3 and MS4, respectively. The difference in VWC between Mix 6 and Mix 6-SR1.0 might be partially attributed to the different overlay construction time (Mix 6 on 7/22/2016 and Mix 6-SR1.0 on 8/29/2016), since the early age exposure condition could have a significant impact on moisture condition in the concrete.

(5) As shown in Figs. 14(c) and 14(d), Mix 8 reached a stable VWC before 100 days after its

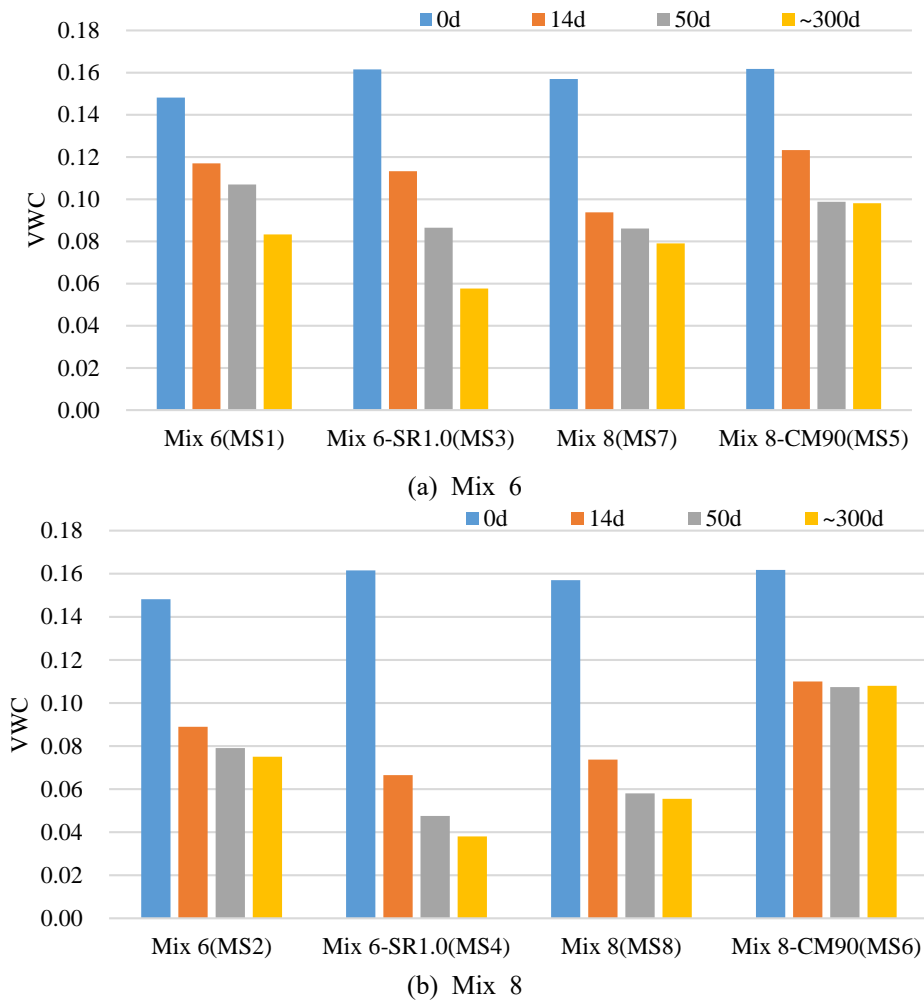


Fig. 15 Comparison of MS readings at 0, 14, 50, and ~300 days of field monitoring

overlay construction, and the stable VWC values of Mix 8 were 0.082 and 0.058 for MS7 and MS8, respectively. Comparing with Mix 8, Mix 8-CM90 had a quite different moisture behavior, especially in the location away from the joint/abutment (MS6). MS6 readings (Fig. 14(d)) show that the concrete had a very rapid moisture drop before 14 days, and reached a relatively high stable VWC value (0.108) shortly thereafter. Such a behavior might be attributed to the pore structure of the concrete, which needs further study. The reduced free drying shrinkage might also be responsible for the relatively high VWC value.

Fig. 15 illustrates that concrete at the location away from the abutment had a sharp moisture decrease in the first 14 days, which might be largely contributed by cement hydration. All VWC curves exhibited a daily fluctuant trend throughout the entire sensor monitoring period. This fluctuation was probably due to environmental moisture change during day and night as well as weather changes.

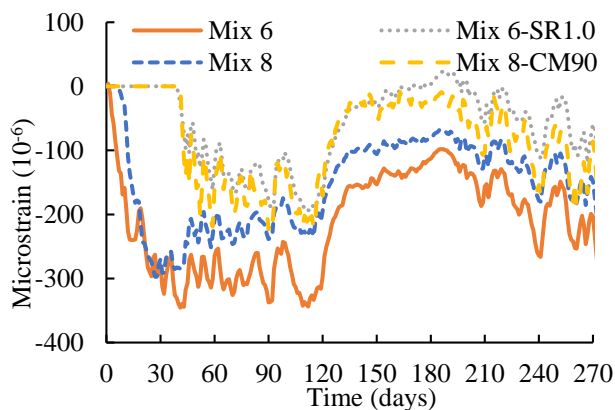


Fig. 16 Microstrain at mini slabs for different mixes

5.5 Strains of mini slabs

To further understand the field concrete shrinkage behaviour under unrestraint condition, the strains in mini slab samples were studied. As seen in Fig. 11, the strain gauges in the mini slabs were in the longitudinal direction. Fig. 16 illustrates the microstrain monitored by the strain gauges in the mini slabs. It indicates that mini slabs were mainly subjected to compressive strains due to concrete shrinkage under an unrestrained condition. As the slabs were under the bridge deck, their thermal expansion at the summer time in the early age was much less than concrete overlays, and therefore, free drying shrinkage was the dominate deformation. During the winter time, the mini slabs expanded against freezing temperature, which offset the shrinkage and reduce the compressive strain. With temperature rising, such expansion reduced, and compressive strain increased until the second summer. Fig. 17 also reveals that the mini slabs of modified mixes had the much less compressive strains caused by free shrinkage than their original mixes. This is consistent with the laboratory shrinkage test results presented in Fig. 13.

5.6 Strains of bridge overlays

In Fig. 4, for each mix, four strain gauges were installed transversely (perpendicular to the traffic direction) in the overlay with a distance of 90 cm to 2270 cm from the abutment. One strain gauge was installed longitudinally (parallel to the traffic direction) with a distance of 2270 cm from the abutment. Figs. 17 and 18 show the strains of all overlay mixes (positive: tension and negative: compression).

It should be noted that the strains measured in the field concrete decks resulted from the combined effects of hydration (autogenous shrinkage), drying-wetting cycles, and thermal expansion/contraction, traffic loads, and creep behavior. The concrete of the bridge decks was under a strained condition. From Fig. 17 and Fig. 18, the following observations can be made:

(1) The strain ranged within -50 to +150 microstrain for all strain gauges embedded in overlays, which was in typical range from -150 to +150 microstrain in response to environmental loads, similar to those found in studies (Wells 2005, Asbahan 2009, Qin 2011, Nassiri 2011).

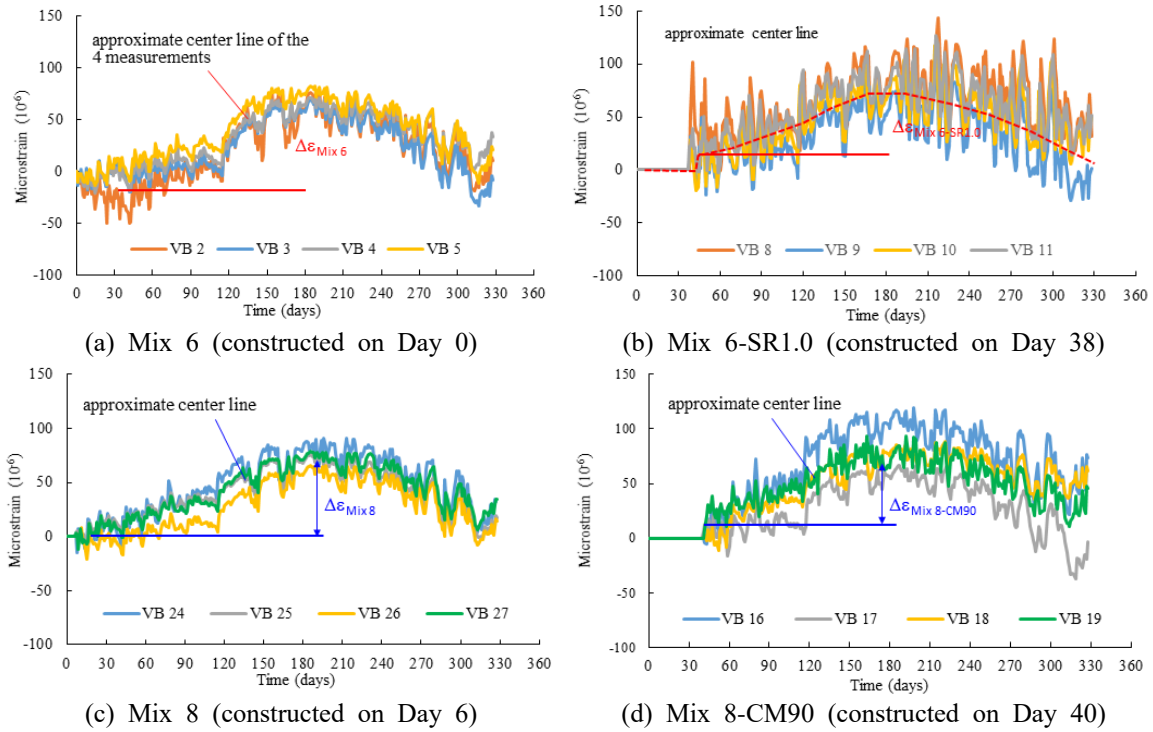


Fig. 17 Strain gauge readings at various locations of overlays in the transverse direction

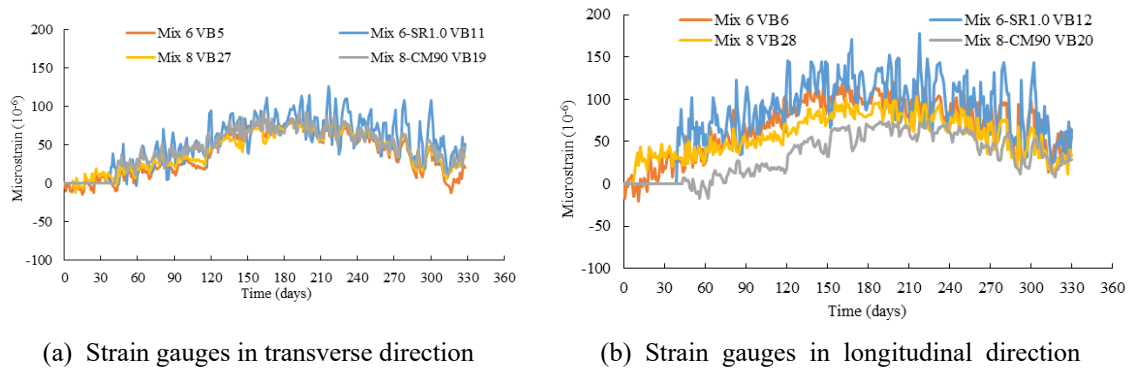


Fig. 18 Comparison of strains in different concrete mixes

(2) The shapes of all the strain curves were similar, but opposite to that of the ambient temperature curve in Fig. 13. For all mixes, the highest tensile strains (shrinkage) encountered in the wintertime (around Day 180). Some compressive strains (expansion) were observed in the summertime (around Day 0 and Day 330). This indicates that the thermal strain was dominant in the concrete. The overlay of Mix 6 displayed more compressive strains, due to the highest cement content, highest heat of hydration, and the hottest day on construction.



Fig. 19 Crack survey using wet test method (water wetting of concrete surface)

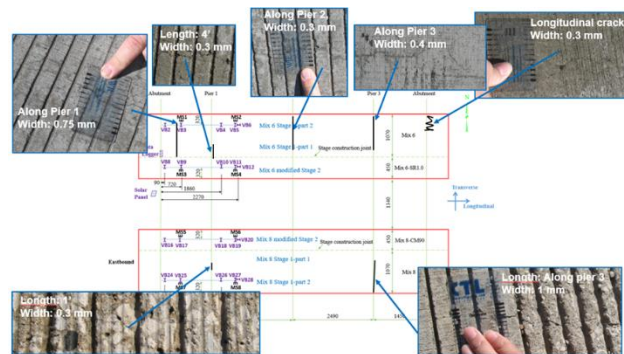


Fig. 20 Cracks on surface of deck after one year of the new overlay in service

(3) All the strain curves also exhibited fluctuations, in corresponding to the ambient temperature curve. However, it was noticed that Mix 6-SR1.0 had the largest daily strain fluctuations (in both transverse and longitudinal sensor readings). Further study is needed to confirm whether it is related to SRA addition.

(4) For a given concrete mix, the strain readings from the sensors in the transverse direction of the bridge were close and independent with their locations. This is because in the view of the transverse cross section, the concrete deck was all supported by the same girders, regardless its distance from the abutment. However, the strain readings of VB2-VB5 were different as seen in Fig. 17. The transverse strain readings in the overlays made with original mixes (Figs. 17(a) and 17(c), Mixes 6 and 8), were very similar, regardless of location. These two overlays were constructed at relatively high ambient temperature ($>25^{\circ}\text{C}$ during the first 7 days). The transverse strain readings from the overlays made with modified mixes (Figs. 17(b) and 17(d), Mixes 6-SR1.0 and 8-CM90) at the different locations displayed quite different. These two overlays were paved at the lower ambient temperature (mostly $<25^{\circ}\text{C}$ during the first 7 days). This may imply that weather condition and concrete maturity at early age might have significant impact the strain behavior of the concrete.

(5) To filter the effect the variations from the strain readings of the transverse strain gauges in different locations for a given mix, an approximate centerline was drawn for each mix (Fig. 17).

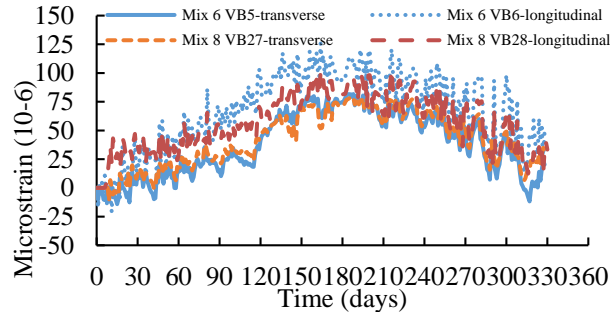


Fig. 21 Strain in different direction at same location

Comparing the centerline curves, it is found that although mini slab study shows Mix 6 had the highest shrinkage among all mixes, the maximum tensile strain from the average of 4 transverse strain gauges (Fig. 17(a)) appeared lower than that of Mix 6-SR1.0. It is because Mix 6 had a compressive (negative) strain, due to the concrete expansion caused by heat of hydration and hot weather at early age, and the tensile strain from the drying and frosting shrinkage compensated the compressive strain. As a result, the absolute strain difference ($\Delta\varepsilon$) was the highest for Mix 6 among all mixes studied. Mix 8 had the second highest $\Delta\varepsilon$. Mix 8-CM90 and Mix 6-SR1.0 had similar $\Delta\varepsilon$ values. This trend is consistent with the order of strains of minislabs.

Fig. 19 compares the strains in different concrete mixes at the locations of 2270 cm from the abutment in both transverse and longitudinal directions. It illustrates that the concrete strain behaviors were generally similar in the transverse direction, although the strain in Mix 6-SR1.0 concrete was a little high. However, for the strains in the longitudinal direction (Fig. 18(b)), the concrete strains in Mixes 6 and 6-SR1.0 were clearly higher than those in Mixes 8 and 8-CM90.

The strains in the longitudinal direction were noticeably larger than the strains in the transverse direction. These indicate that Mixes 6 or 6-SR1.0 might have high potential of cracking in the transversal direction. However, as mentioned previously, cracking potential is related not only to the strain values but also many other parameters, e.g., the concrete tensile strength and creep behavior, and more stress analyses should be conducted to verified the overlay cracking potential. It would be desirable if more strain gauges were installed in the longitudinal direction of each concrete mix.

5.7 Crack survey after the repaired bridge in service for one year

On October 9, 2017, cracks on the surface of overlays that had one year traffic service were surveyed using wet test method. Water was sprayed on concrete surface followed by vacuuming to expose cracks clearly as seen in Fig. 19. Fig. 20 shows the locations and patterns of the cracks. As seen from the figure, five cracks on Mix 6 overlay and two cracks on Mix 8 overlay were observed. The width of cracks was from 0.3 mm to 1mm. They were mostly transverse and located close to piers, possibly due to negative bending moments at the supports. No visible cracks were found on either of the modified mixes (Mix 6-SR1.0 and Mix 8-CM90). These observations supported the strain results of mini slabs as shown in Fig. 16.

The strain measurements from the same location of overlay where cracks were observed were

drawn out to compare the strain magnitude at different directions as shown in Fig. 21. It can be seen that the sensors in longitudinal direction have more strain than those in transverse direction which means that the longitudinal strain is greater than transverse strain. This phenomenon can perfectly explain that the most cracks found on overlays are in transverse.

6. Conclusions

- Modified mixes performed much better than original mixes in traffic service. No cracks occurred in modified mixes after one-year traffic open.
- The exposed cracks on original mixes were all in transverse direction which matched the observation from vibrating wires that longitudinal strain was greater than transverse strain.
- The strain yielded in concrete overlay was the entire effect of concrete shrinkage and restriction, weather and seasonal changes, and traffic load. This comprehensive effect tends to be extensive in field concrete.
- The moisture profiles developed from the data monitoring accurately reflected moisture changes with time starting from paving. It shows that moisture content was mainly consumed at early age due to hydration and it also fluctuated on weather changes and finally stayed constant.
- The calibration of moisture sensor needs to be done for each concrete mix, which is complex to perform. We would prefer to develop a model to do the calibration based on sufficient data. Meanwhile, the inspection period for the sensor-instrumented HPC overlays is only 1 year, and the condition of overlay could be monitored for a longer period in future study.

Acknowledgments

The present study is a part of a research project, Investigation into Shrinkage of High-Performance Concrete Used for Iowa Bridge Decks and Overlays - Phase II Shrinkage Control and Field Investigation, sponsored by the Iowa Department of Transportation. (IHRB Project TR-690).

References

- Afrouhsabet, V. and Teng, S. (2020), "Experiments on drying shrinkage and creep of high performance hybrid-fiber-reinforced concrete", *Cement Concrete Compos.*, **106**. <https://doi.org/10.1016/j.cemconcomp.2019.103481>.
- Asbahan, R.E. (2009), "Effects of the built-in construction gradient and environmental conditions on jointed plain concrete pavements", Ph.D. thesis, University of Pittsburgh.
- ASTM (2017), Standard test method for length change of hardened hydraulic-cement mortar and concrete. ASTM C157. West Conshohocken, PA: ASTM.
- ASTM (2018), Standard test method for compressive strength of cylindrical concrete specimens. ASTM C39. West Conshohocken, PA: ASTM.
- ASTM (2019), Standard specification for chemical admixtures for concrete. ASTM C494. West Conshohocken, PA: ASTM.
- Bahrani, N., Blanc, J., Hornych, P. and Menant, F. (2020), "Alternate method of pavement assessment using

- geophones and accelerometers for measuring the pavement response”, *Infrastructures*, **5**(3), 25. <https://doi.org/10.3390/infrastructures5030025>.
- Barroca, N., Borges, L., Velez, F., Monteriro, F., Gorski, M. and Castro-Gomes, J. (2013), “Wireless sensor networks for temperature and humidity monitoring within concrete structures”, *Constr. Build. Mater.*, **40**, 1156-1166. <https://doi.org/10.1016/j.conbuildmat.2012.11.087>.
- Buenfeld, N., Davis, R., Karmini, A. and Gilbertson, A. (2008), *Intelligent monitoring of concrete structures*, UK: CIRIA.
- Chung, H.W., Subgranon, T. and Tia, M. (2020), “Reducing cementitious paste volume of slipformed pavement concrete by blending aggregates”, *Int. J. Pavement Res. Technol.*, **13**, 679-685. <https://doi.org/10.1007/s42947-020-6002-9>.
- Dong, W., Zhao, X., Zhou, X. and Yuan, W. (2019), “Effects of moisture gradient of concrete on fracture process in restrained concrete rings: Experimental and numerical”, *Eng. Fract. Mech.*, **208**, 189-208. <https://doi.org/10.1016/j.engfracmech.2019.01.011>.
- Ghafoori, E., Hosseini, A., Al-Mahaidi, R., Zhao, X.L. and Motavalli, M. (2018), “Prestressed CFRP-strengthening and long-term wireless monitoring of an old roadway metallic bridge”, *Eng. Struct.*, **176**, 585-605. <https://doi.org/10.1016/j.engstruct.2018.09.042>.
- Hansen, W. and Wei, Y. (2008), PCC pavement acceptance criteria for new construction when built-in curling exists. Research Report RC-1481. Michigan Department of Transportation, Lansing, MI.
- James, J. and John, E. (2020), *The effectiveness of shrinkage reducing admixture and fly ash on plastic shrinkage of concrete*, UK: CRC Press.
- Klausen, A. and Kanstad, T. (2021), “The effect of shrinkage reducing admixtures on drying shrinkage, autogenous deformation, and early age stress development of concrete”, *Struct. Concrete*, **22**, 596-606. <https://doi.org/10.1002/suco.201900583>.
- Ma, L., Zhao, Y. and Gong, J. (2018), “Restrained early-age shrinkage cracking properties of high-performance concrete containing fly ash and ground granulated blast-furnace slag”, *Constr. Build. Mater.*, **191**, 1-12. <https://doi.org/10.1016/j.conbuildmat.2018.09.154>.
- Mccarter, W. and Vennesland, O. (2004), “Sensor systems for use in reinforced concrete structures”, *Constr. Build. Mater.*, **18**(6), 351-358. <https://doi.org/10.1016/j.conbuildmat.2004.03.008>.
- Min, H., Zhang, W. and Gu, X. (2018), “Effects of load damage on moisture transport and relative humidity response in concrete”, *Constr. Build. Mater.*, **169**, 59-68. <https://doi.org/10.1016/j.conbuildmat.2018.02.203>.
- Nassiri, S. (2011), “Establishing permanent curl/warp temperature gradient in jointed plain concrete pavements”, Ph.D. thesis, University of Pittsburgh.
- Ni, Y.Q., Hua, X.G., Fan, K.Q. and Ko, J.M. (2005), “Correlating modal properties with temperature using long-term monitoring data and support vector machine technique”, *Eng. Struct.*, **27**(12), 1762-1773. <https://doi.org/10.1016/j.engstruct.2005.02.020>.
- Norris, A., Saafi, M. and Romine, P. (2008), “Temperature and moisture monitoring in concrete structures using embedded nanotechnology/microelectromechanical systems (MEMS) sensors”, *Constr. Build. Mater.*, **22**(2), 111-120. <https://doi.org/10.1016/j.conbuildmat.2006.05.047>.
- Qin, Y. (2011), “Numerical study on the curling and warping of hardened rigid pavement slabs”, Ph.D. thesis, Michigan Technological University.
- Rao, S. and Roesler, J. (2005), Characterization of effective built-in curling and concrete pavement cracking on the palmdale test sections. Pavement Research Center, Institute of Transportation Studies, University of California, Berkeley, CA.
- Ray, I., Gong, Z., Davalos, J.F. and Kar, A. (2012), “Shrinkage and cracking studies of high performance concrete for bridge decks”, *Constr. Build. Mater.*, **28**(1), 244-254. <https://doi.org/10.1016/j.conbuildmat.2011.08.066>.
- Rice, J. (2014), Optimization of a pavement instrumentation plan for a full-scale test road: evaluation. Final report, Florida Department of Transportation, FL, BDV31-977-04.
- Shen, D., Jiang, J., Zhang, M. and Yao, P. (2018), “Tensile creep and cracking potential of high performance concrete internally cured with super absorbent polymers at early age”, *Constr. Build. Mater.*, **165**, 451-

461. <https://doi.org/10.1016/j.conbuildmat.2017.12.136>.
- Shen, D.J., Wang, W.T., Liu, J.W., Zhao, X.G. and Jiang, G.Q. (2018), "Influence of Barchip fiber on early-age cracking potential of high performance concrete under restrained condition", *Constr. Build. Mater.*, **187**, 118-130. <https://doi.org/10.1016/j.conbuildmat.2018.07.121>.
- Wang, K., Schlorholtz, S., Sritharan, S., Seneviratne, H., Wang, X. and Hou, Q. (2013), "Investigation into shrinkage of high-performance concrete used for iowa bridge decks and overlays", In *Trans Project Reports*, 22.
- Wei, Y. and Hansen, W. (2011), "Characterization of moisture transport and its effect on deformations in jointed plain concrete pavement", *Transportation Research Record: J. Transport. Res. Board*, **2240**(1), 9-15. <https://doi.org/10.3141/2240-02>.
- Wells, S. (2005), "Early age response of jointed plain concrete pavements to environmental loads", Master. Thesis, University of Pittsburgh, PA.
- Wu, L., Farzadnia, N., Shi, C., Zhang, Z. and Wang, H. (2017), "Autogenous shrinkage of high performance concrete: A review", *Constr. Build. Mater.*, **149**, 62-75. <https://doi.org/10.1016/j.conbuildmat.2017.05.064>.
- Wu, X., Dong, Z., Sun, L. and Jia, T. (2022), "Experimental study of the volume drying shrinkage characteristics of lignite under low temperatures", *ACS Omega*, **7**, 12. <https://doi.org/10.1021/acsomega.1c05575>.
- Yang, S., Shen, K., Ceylan, H., Kim, S., Qiao, d. and Gopalakrishnan, K. (2015), "Integration of a prototype wireless communication system with micro-electromechanical temperature and humidity sensor for concrete pavement health monitoring", *Cogent Eng.*, **2**, 1014278. <http://dx.doi.org/10.1080/23311916.2015.1014278>.
- Yuan, T.F., Kim, S.K., Koh, K.T. and Yoon, Y.S. (2018), "Synergistic benefits of using expansive and shrinkage reducing admixture on high-performance concrete", *Materials*, **11**(12). <https://doi.org/10.3390/ma11122514>.